Int. J. Electrochem. Sci., 15 **(2020)** 10058 – 10080, doi: 10.20964/2020.10.23

International Journal of
ELECTROCHEMICAL
SCIENCE
www.electrochemsci.org

Inhibition Synergism Between Alkyl Imidazoline and Potassium Iodide on the Corrosion of Carbon Steel in Citric Acid Solution

Jianjia Shen, Yaqiong Chen, Yitong Tan, Dong Yang, Xinxin Liu, Zesong Gao and Qiangqiang Liao[*]

Shanghai Engineering Research Centre of Heat-Exchange System and Energy Saving, Shanghai Key Laboratory of Materials Protection and Advanced Materials in Electric Power, Shanghai University of Electric Power, Shanghai 200090, China
[*]E-mail: liaoqianqiang@shiep.edu.cn

Received: 4 May 2020 / *Accepted:* 17 July 2020 / *Published:* 31 August 2020

The synergistic inhibition effect of the complex of 2-undecyl-N-carboxymethyl-N-hydroxyethly imidazoline (UHCI) and potassium iodide (KI) on the corrosion of 45# carbon steel subjected to 4 wt.% citric acid solution is explored by weight loss testing, electrochemical measurement, and X-ray photoelectron spectroscopy (XPS) analysis. Based on the weight loss test, 94.15% inhibition capacity is obtained by compound inhibitors (UHCI:KI=30:10) after immersion in 4 wt.% citric acid for 8 h, which is consistent with the results from electrochemical technology. The discussion extends to the effects of temperature and immersion time to achieve the ideal inhibition performance for further protection. The adsorption of the studied compound fitted well with the Langmuir isotherm model. The XPS analysis confirms physical and chemical interactions between the UHCI/KI complex inhibitors and metal surface to defend the aggressive electrolyte. Additionally, the corrosion inhibition mechanism of UHCI inhibitor in the presence of iodine ions in the citric acid solution is discussed.

Keywords: Carbon steel; Corrosion inhibitor; Synergism; EIS; XPS.

1. INTRODUCTION

45-grade medium carbon steel in a tempered and quenched condition is widely employed as a structural mechanical material in the thermal industry. Induced by dissolved oxygen in the boiler water, generated steam, deposits generated by scale, local mechanical stress, etc., the active pipeline will be subjected to corrosive behaviour resulting in the formation of corrosion products after long-term service of the boiler [1]. Once the corrosion products accumulate to a certain extent without removal, the heat transfer efficiency of boiler will drop sharply, which leads to local overheating and the possibility of tube explosion accidents [2]. Up to now, acid solutions like hydrochloric acid, sulphuric acid,

aminosulfonic acid, and citric acid are widely used to remove undesirable products [3]. During the pickling process of the boiler, not only the scale and iron oxides can be eliminated but also a certain amount of metal will be re-corroded by chemical reaction. Accordingly, incorporating the corrosion inhibitor species in the pickling agent has been proposed as one of the economical and reliable ways for mitigating the corrosion [4]. Corrosion inhibitors can be divided into two categories: inorganic and organic corrosion inhibitors. Inorganic inhibitors can mitigate damage to the metal surface by passivation or forming a deposit to isolate the interface, while organic inhibitors play the inhibitory role by activated absorption with heteroatoms and double bonds [5]. The capacity of corrosion inhibition depends on multiple factors, e.g. microstructure and state of the metal surface, environmental conditions, and the characteristics and dosage of the inhibitor.

Imidazoline derivatives have been developed by corrosion researchers thanks to their low toxicity, simple preparation, and excellent corrosion inhibition efficiency. Zhang et al. reported that 2-methyl-4-phenyl-1-tosyl-4,5-dihydro-1H-imidazole (IMI) weakened the corrosion rate of P110 carbon steel in a 1.0 M HCl solution [6]. Zuo et al. studied the corrosion inhibition effects of thioureido imidazoline on the pitting corrosion of X70 steel in an NaCl-$NaNO_2$ solution [7]. Li et al. revealed that imidazoline inhibitor efficiently retarded the crevice corrosion of N80 carbon steel in CO_2-NaCl acetic solution when added at the beginning [8]. Gouron et al. studied the corrosion inhibition mechanism of various imidazoline-based inhibitors on iron oxide with DFT calculations, and explored the influence of alkyl length [9]. Yu et al. synthesised the symmetric imidazoline inhibitor (DBI) and pointed out that the inhibition strengthened with increasing of inhibitor concentration under 1 M HCl conditions [10]. Xiang et al. compared imidazoline with piperazine regarding suppression of the corrosion of N80 steel in supercritical CO_2 phase and aqueous phases, and found that piperazine outperformed imidazoline inhibitor [11]. Solomon et al. found that N-(2-(2-tridecyl-4,5-dihydro-1H-imidazol-1-yl)ethyl) tetradecanamide (NTETD) with 300 mg/L achieved 93% inhibition efficiency for low carbon steel in a 15% HCl solution [12].

Nevertheless, a single inhibitor to mitigate metal corrosion may not ideal in some electrolyte solutions. Researchers have found that the compound inhibitors with synergistic effects are an alternative to solve this problem, which improves both the inhibition performance and reduces the dosage of inhibitor. Yuan et al. determined the synergistic inhibition effect of dipropargyl methoxythiourea imidazoline (DPFTAI) and pyridine quaternary ammonium salt (16BD) by simulation calculation [13]. Qian et al. studied the synergism efficiency of imidazoline and sodium dodecylbenzenesulphonate (SDBS) inhibitors on corrosion inhibition of X52 carbon steel susceptible to CO_2-saturated chloride solutions [14]. Han et al. studied the inhibition capacity of imidazoline-base inhibitor mixtures (IMB and IMO) on the corrosion of L245 steel in HCl solution through experimental and theoretical methods [15]. Many studies have found that halide ions can also enhance the inhibitory performance of corrosion inhibitors by strengthening the adsorption of the inhibitors on metal surfaces [16,17]. Cao et al. discovered that novel ionic liquid and synergistic halide additives KI, worked against corrosion effectively for the protection of carbon steel in 0.5 M HCl solution, and the maximum inhibition efficiency was in the range 94.8%-96.2% [18]. Wei et al. discovered that the introduction of KI substantially decreased the corrosion rate in the supercritical CO_2 environment with an imidazoline inhibitor [19]. The synergistic influence of KI at various concentrations of Schiff base 1 (Dapsone-

benzaldehyde), Schiff base 2 (Dapsone-salicylaldehyde) inhibitors, and three dihydropyrimidinone (DHPM) derivatives were investigated by Singh et al [20,21]. It has been proved that 2-heptadecyl-1-[2-(octadecanoylamino)ethyl]-2-imidazoline (QSI) with -$C_{17}H_{35}$ addition of KI synergistically enhanced the inhibition performance to approximately 90% in an acidic environment [22].

Most of the literature on corrosion inhibitors mainly focusses on inorganic acid detergents such as hydrochloric acid and sulphuric acid. Regrettably, similar research is rather limited for weak organic acids e.g. citric acid ($C_6H_8O_7$), amidosulfuric acid (NH_2SO_3H), and even more complex agents [23]. Some reports have even pointed out that citric acid can also act as a corrosion inhibitor to achieve the protection of metals [24]. The main driving force behind this study was to explore an environmentally friendly inhibitor towards steel corrosion in a 4 wt.% citric acid solution, investigate the synergistic inhibition action with various concentrations of KI, and study the effect of temperature and immersion time to achieve the ideal protection performance. As a non-toxic, non-irritant, and biodegradable green organic compound, 2-undecyl-N-carboxymethyl- N-hydroxyethly imidazoline (UHCI) is widely used in baby shampoo, body wash and other cleaning substances. In this study, the capacity of corrosion inhibition of a UHCI and KI composite inhibitor was studied by weight loss measurement and electrochemical technology. XPS analysis was applied to identify the physical and chemical interactions between the complex UHCI/KI and the carbon steel surface.

2. EXPERIMENTAL METHODS

2.1 Preparation of solutions and materials

The 2-undecyl-N-carboxymethyl-N-hydroxyethyl imidazoline (UHCI) corrosion inhibitor used in this work was purchased from Shanghai Fakai Chemical Co., Ltd. The structural formula is shown in Fig. 1. The total solid content of UHCI is 40 ± 2.0 %, and it was used as the raw material without further purification. Potassium iodide was purchased from Shanghai Aibi Chemistry Preparation Co., Ltd. Aggressive solutions were prepared with 4 wt.% citric acid in the absence and presence of different ratios of UHCI and KI according to the chemical cleaning guide for steam power plant-DL/T 794-2001. The composition of carbon steel 45# is shown in the Table 1.

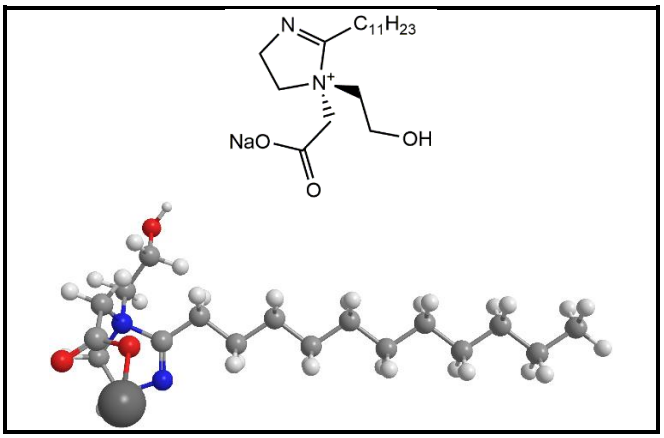

Figure 1. The chemical structure of UHCI.

Table 1. Chemical composition of 45# carbon steel (wt.%).

Elements	C	Si	Mn	Cr	Ni	Cu	Fe
Content (%)	0.42-0.50	0.17-0.37	0.50-0.80	≤ 0.25	≤ 0.30	≤ 0.25	Balance

2.2 Weight loss tests

Carbon steel 45 # was cut into rectangular sheets (50 ± 0.1 mm × 25 ± 0.1 mm × 2 ± 0.1 mm), then emery paper was used (grade 180 up to 1200) to polish the steel coupons. The samples were then rinsed by deionised water, absolute ethanol and acetone, in order. Finally, the sample weight (m_1) was measured and then the samples were stored in a moisture-free desiccator. After immersing the steel sheet in the corrosive medium for 8 hours, a soft eraser was used to remove surface attachments, then the sample was rinsed again and reweighed (m_2) after drying. Three trials in parallel were required. The mass change before and after metal corrosion was used to calculate the metal corrosion rate (v) and the inhibition efficiency (η_{wL}%).

$$v = \frac{m_1 - m_2}{S \cdot t} \quad (1)$$

where S is the area of metal exposed to the aggressive electrolyte, and t is the immersion time (h).

$$\eta_{wL} = \frac{v_0 - v}{v_0} \times 100\% \quad (2)$$

where v_0 and v are for the corrosion rates with and without corrosion inhibitor, respectively.

2.3 Electrochemical measurements

Electrochemical testing was based on the classical three electrode system: ∅1.0 cm carbon steel 45# cylindrical rods with an effective area of 0.78 cm^2 were used for the working electrode, a saturated calomel electrode (SCE) and a platinum electrode were used as the reference electrode and auxiliary electrodes, respectively. The instrument used was a VersaSTAT3 electrochemical workstation from US Princeton applied research company. The fitting and related parameters were obtained through the Zview software package. The non-working surface was sealed with epoxy resin. The working electrode surface was polished, step by step, using emery papers with different degrees of roughness (180 up to 1200 grit). The sample was flushed by DI water and absolute ethyl alcohol before drying. The sample was then immersed in the prepared corrosion solutions for 4 h. The polarisation curve was measured from -900 mV to -100 mV at a scanning rate of 5 $mV \cdot s^{-1}$. The EIS results were achieved over a frequency range between 0.05 Hz and 100 kHz with 5 mV amplitude. Three electrochemical experiments were repeated to obtain good reproducibility. The Eqs. (3) and (4) were used for determining the corrosion inhibition efficiency based on polarisation (η_p%) and EIS (η_R%) results [25]:

$$\eta_p = (1 - \frac{I_{corr}}{I_{corr}^0}) \times 100\% \quad (3)$$

$$\eta_R = (1 - \frac{R_{ct}^o}{R_{ct}}) \times 100\% \quad (4)$$

where I_{corr} and I_{corr}^0 are the corrosion current densities with and without corrosion inhibitor, respectively. Similarly, the parameters R_{ct} and R_{ct}^o refer to the charge transfer resistance with and without corrosion inhibitor.

2.4 X-ray photoelectron spectroscopy

To determine the elemental content and valence state of the adsorbed layer on the surface of the 45# carbon steel, XPS measurements were carried out using a Perkin-Elmer PHI 5000C ESCA spectrometer (USA) with monochromatic Mg-Kα radiation ($h\nu$ = 1253.6 eV) as the X-ray source. The pass energy was fixed at 23.5, 46.95 or 93.90 eV to ensure sufficient resolution and sensitivity, and the X-ray anode was run at 300 W and the high voltage was kept at 14.0 kV with a detection angle at 45°. The C 1*s* peak at 284.6 eV (binding energy) was used as the internal reference in order to compensate for charge effects occurring during the charge shift. The pressure was in the 10^{-8} Torr range during the experiments and XPSPeak41 software was used for all data processing. Prior to XPS analysis, the 45# carbon steel samples were immersed in the citric acid solution both with and without inhibitor for 4 h at 298 K, then rinsed with ethanol and DI water followed by air drying at room temperature.

3. RESULTS AND DISCUSSION

3.1. Weight loss test

The corrosion rate of the carbon steel test piece in 4% (wt.%) citric acid solution without inhibitors was 1.538 g/(m^2·h) over 8 hours. As shown in Table 2, compared with the blank solution, the corrosion inhibition effect of the UHCI-KI mixture was better than each of the individual components regarding the total inhibitor concentration constant. The UHCI-KI inhibitor showed a stable and higher lever corrosion inhibition effect over the ratios of 35:5, 30:10, 25:15. When the ratio of UHCI to KI was 30:10, the corrosion inhibition efficiency reached a maximum of 94.15%. Hence, it can be seen that potassium iodide and UHCI had a synergistic effect on the corrosion inhibition of 45# carbon steel in the citric acid solution.

Table 2. Corrosion rate (v) and the inhibition efficiency (η_{wL}%), calculated results of carbon steel with different ratios of inhibitors in 4 wt.% citric acid solution after 8 hours immersion from the weight loss test: (a) Blank; (b) 0.4% KI; (c) 0.4% UHCI; (d) 0.35% UHCI and 0.05% KI; (e) 0.3% UHCI and 0.1% KI; (f) 0.25% UHCI and 0.15% KI.

UHCL:KI	v (g·m^{-2}·h^{-1})	η_{wL} (%)
Blank	1.538	-
0.4%KI	0.409	73.41

0.4%UHCI	0.165	89.27
35:5	0.103	93.30
30:10	0.090	94.15
25:15	0.094	93.89

3.2. Potentiodynamic polarisation measurements

Fig. 2 shows the polarisation curves of 45 # carbon steel immersed in the 4% citric acid solutions with blank, and different contents of corrosion inhibitors, after 4 h immersion. The electrochemical parameters of the polarisation curve data, listed in Table 3, correspond to the E_{corr} (corrosion potential), I_{corr} (corrosion current density), β_a (anodic Tafel slopes), β_c (cathodic Tafel slopes) and η_p% (the corrosion inhibition efficiency based on polarisation). It can be seen from Fig. 2 that compared with the absence of the inhibitor, the corrosion potential of the carbon steel electrode E_{corr} shifted positively after the addition of the inhibitor. At the same time the corrosion current density I_{corr} declined significantly. It is worth noting that the obtained I_{corr} was lower with the mixed inhibitors than when KI or UHCI were added alone, which indicates that there is a synergistic effect of corrosion inhibition between UHCI and KI. According to Fig. 2, both the anodic and cathodic current densities drifted to lower values at different ratios of UHCI and KI. This phenomenon can be used as evidence that the composite inhibitors have inhibitory effects on both the anode and cathode reactions [26]. In detail, all the cathodic polarisation curves with different inhibitors were parallel to that of the blank sample, which means that there is the same cathodic reaction mechanism for the carbon steel in the citric acid. Additionally, the plots of the anodic branches have obviously changed which indicates that the inhibitors formed a barrier film on the metal surface that resists the iron dissolution behaviour [27].

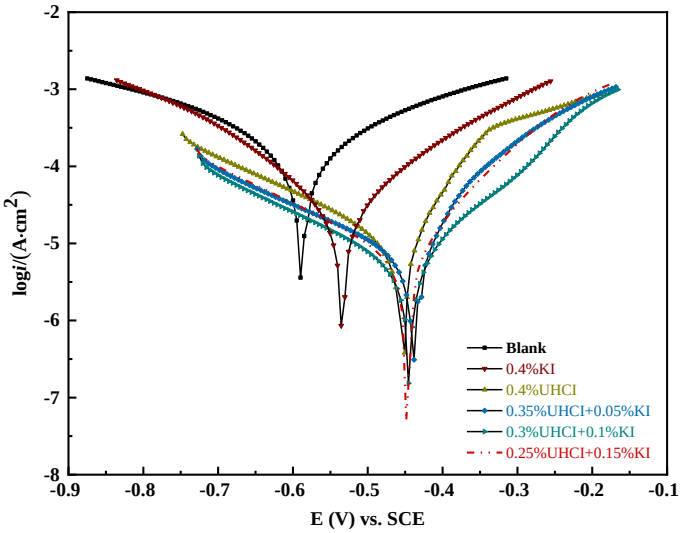

Figure 2. Electrochemical polarisation curves of carbon steel measured with different ratios of inhibitors in 4% citric acid solution after 4 h immersion: (a) Blank; (b) 0.4% KI; (c) 0.4% UHCI; (d) 0.35% UHCI and 0.05% KI; (e) 0.3% UHCI and 0.1% KI; (f) 0.25% UHCI and 0.15% KI.

According to the data shown in Table 3, 0.4 wt.% KI solution as a mixed-type corrosion inhibitor in this aggressive environment owing to the corrosion potential displacement of less than 80 mV [28]. In other words, the remaining complex corrosion inhibitors of different compositions tend to be anodic type corrosion inhibitors as shown by the positive shift of the corrosion potential and the significantly changed anodic branch shapes [29]. Notably, compared to the blank solution, the value of β_a decreases and the value of β_c generally increases in the presence of inhibitors with different ratios, which concurs with the results found in the literature [10,18,30]. The Tafel slopes exhibit an irregular characteristic with different concentrations of complex inhibitors. This can be correlated with the complexity of the adsorption and desorption processes of the active species in the solution, and the blocking mechanism of the cathode and anode reaction sites. Beginning with the increase of the concentration of KI, the corrosion inhibition efficiency η_p% increases slightly until reaching a maximum of 94.24%. As a result, it can be considered that the optimal ratio of UHCI to KI is 3:1. Moreover, it is widely accepted that cathodic reaction for carbon steel in an acid solution is the hydrogen evolution reaction as follows [31]:

$$Fe + H^+ \leftrightarrow (FeH^+)_{ads} \quad (5)$$
$$(FeH^+)_{ads} + e^- \longrightarrow (FeH)_{ads} \quad (6)$$
$$(FeH)_{ads} + H^+ + e^- \longrightarrow Fe + H_2 \quad (7)$$

The anodic reactions are described the following dissolution mechanism steps [32,33]:

$$Fe + H_2O \leftrightarrow FeOH_{ads} + H^+ + e^- \quad (8)$$
$$FeOH_{ads} \rightarrow FeOH^+ + e^- \quad (9)$$
$$FeOH^+ + H^+ \leftrightarrow Fe^{2+} + H_2O \quad (10)$$

When iodine ion is added to the solution, it can replace the hydroxyl ion adsorbed on the metal surface owing to low electronegativity, large ionic radius, and high hydrophobicity [20,34]:

$$Fe + H_2O + I^- \leftrightarrow [FeIOH]^-_{ads} + H^+ + e^- \quad (11)$$
$$[FeIOH]^-_{ads} \rightarrow FeIOH + e^- \quad (12)$$
$$FeIOH + H^+ \leftrightarrow Fe^{2+} + I^- + H_2O \quad (13)$$

It is generally believed that the adsorption of corrosion inhibitor molecules on metal surfaces is achieved by replacing already adsorbed water molecules as follows:

$$Inh_{sol} + xH_2O_{ads} \leftrightarrow Inh_{ads} + xH_2O_{sol} \quad (14)$$
$$Fe^{2+} + Inh_{ads} \leftrightarrow [Fe - Inh]^{2+}_{ads} \quad (15)$$

Consequently, with the adsorption of inhibitor molecules, the area of metal exposed to the corrosive medium decreases for the cathode, which reduces the active centres for the hydrogen reduction reaction [35,36]. However, the effect on its mechanism is still small, so the cathode polarisation curve

shows a parallel trend. For the anode, forming a dense passivation film and an adsorption film is one of the effective measures to protect the dissolution of iron ions.

Table 3. Electrochemical fitting parameters obtained from polarisation curves for carbon steel with different ratios of inhibitors in 4% citric acid solution after 4 h immersion.

UHCI:KI	$-E_{corr}$, V *vs* SCE	I_{corr}, μA·cm^{-2}	β_a, mV dec^{-1}	$-\beta_c$, mV dec^{-1}	η_p, %
0	0.593	58.93	122	102	-
0.4% KI	0.534	15.11	101	106	74.36
0.4% UHCI	0.455	7.530	71	172	87.22
39:1	0.468	6.016	74	134	89.79
38:2	0.480	5.951	108	131	89.90
37:3	0.453	5.682	70	165	90.36
36:4	0.484	5.136	104	98	91.28
35:5	0.440	4.600	66	162	92.19
33.5:6.5	0.459	4.486	101	165	92.39
32:8	0.453	4.416	92	159	92.51
31:9	0.445	4.050	88	170	93.13
30:10	0.443	3.392	83	164	94.24
29:11	0.456	3.726	117	149	93.68
28:12	0.452	4.120	88	162	93.01
25:15	0.449	4.332	84	151	92.65

3.3. Electrochemical impedance spectroscopy

Electrochemical impedance spectroscopy can assess the interface changes and interactions of carbon steel with inhibitors adsorption or desorption [37]. The impedance spectra of 45# carbon steel electrode subjected to the inhibitor-free and inhibitor-loaded citric acid solution after 4 hours are given in Fig. 3 and Fig. 4. The diagrams were fitted by the Zsimpwin software, and the relevant calculated parameters are listed in Table 4, including the solution resistance (R_s), the charge transfer resistance (R_{ct}), the constant phase angle element (CPE) which represents the capacitance of the double layer capacitance C_{dl}, the inhibition capacitance (η_R), and the surface coverage degree (θ). The impedance of a CPE is expressed as follows [38]:

$$Z_{CPE} = Y_0^{-1}(jw)^{-n} \quad (16)$$

where Y_0 is a proportional factor, j is an imaginary root ($\sqrt{-1}$), ω is the angular frequency, and n is the deviation parameter (varies from 0 to 1). Moreover, the double layer capacitance (C_{dl}) can be calculated by using the following equation [39]:

$$C_{dl} = Y_0(\omega)^{n-1} = Y_0(2\pi f_{Z_{im-Max}})^{n-1} \quad (17)$$

The impedance spectra in Fig. 3 all show a flattened semicircle due to the electrode surface roughness and heterogenicity. As can be seen from the Nyquist diagram in Fig. 3, all the shapes of curves of inhibited electrodes compared to the uninhibited electrodes, maintain a high degree of similarity, which reveals that the corrosion mechanism of carbon steel remains unchanged. The diameter of the semicircle corresponds to R_{ct}, and the larger the R_{ct}, the better the corrosion inhibition efficiency, which means that there is a protective film formed on the surface of the metal to retard the corrosion reaction. As the KI ratio increases, the diameter of the semicircle initially increases significantly, and then decreases. When the ratio of UHCI to KI was 3: 1, η_R reached a maximum of 95.49%. This is consistent with the conclusions obtained by the weight loss test method and the polarisation curve test method. Fig. 5 represents the equivalent circuit model applied to fit the electrochemical impedance data.

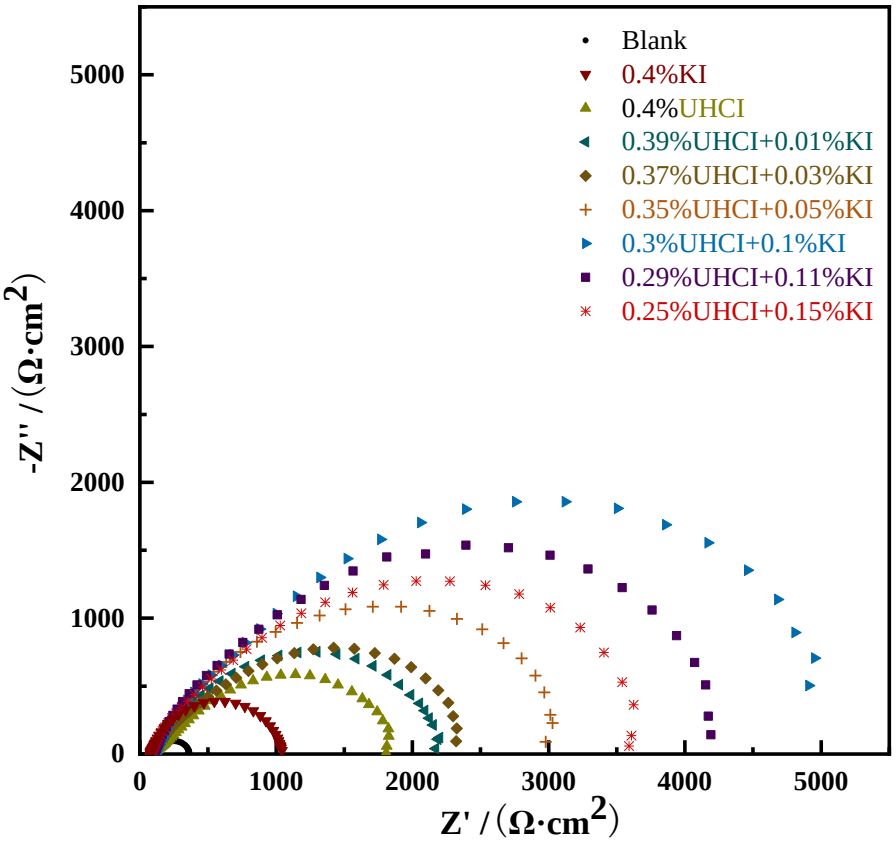

Figure 2. Electrochemical impedance in Nyquist plots of carbon steel measured with different ratios of inhibitors in 4% citric acid solution after 4 h immersion: (a) Blank; (b) 0.4% KI; (c) 0.4% UHCI; (d) the mixture of UHCI and KI.

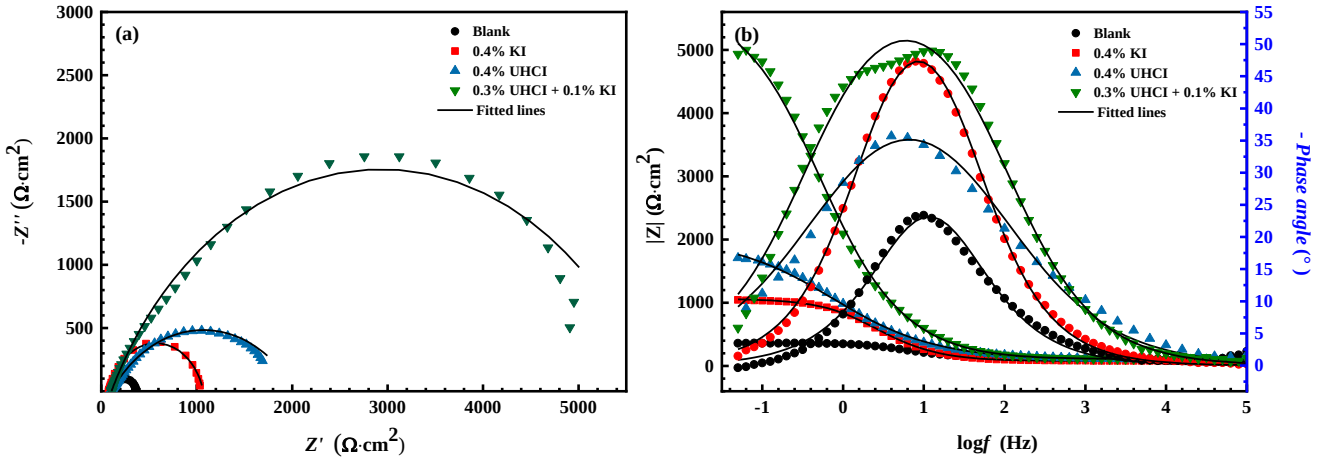

Figure 3. Electrochemical impedance in Nyquist and Bode plots of carbon steel with different ratios of inhibitors in 4% citric acid solution after 4 h immersion: (a) Blank; (b) 0.4% KI; (c) 0.4% UHCI and (d) 0.3% UHCI and 0.1% KI.

Table 4. Electrochemical impedance fitting parameters of 45# carbon steel with different ratios of inhibitors in 4% citric acid solution after 4 h immersion at 298 K.

UHCI:KI	R_s, Ω·cm^2	R_{ct}, Ω·cm^2	CPE_{dl} $(\mu\Omega^{-1}s^n cm^{-2})$	η_R%	θ
0	114.9	254.7	230.5	-	-
0.4%KI	80.23	988.1	132.1	74.22	0.7422
0.4%UHCI	105.4	1802	182.4	85.86	0.8586
39:1	101.6	2280	111.3	88.83	0.8883
38:2	90.61	2537	122.4	89.96	0.8996
37:3	85.99	2664	179.1	90.44	0.9044
36:4	89.84	2953	159.9	91.37	0.9137
35:5	94.60	3239	109.5	92.14	0.9214
33.5:6.5	87.62	3653	78.98	93.03	0.9303
32:8	94.13	4179	106.5	93.90	0.9390
31:9	109.8	4363	83.55	94.16	0.9416
30:10	107.2	5652	99.13	95.49	0.9549
29:11	101.7	4509	90.01	94.35	0.9435
28:12	110.7	4070	110.0	93.74	0.9374
25:15	71.59	4025	112.7	93.67	0.9367

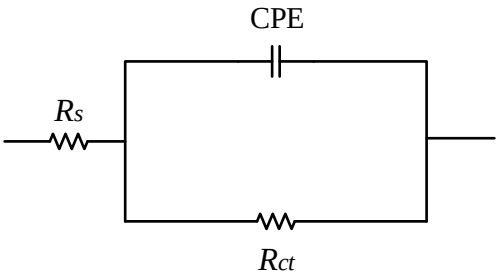

Figure 4. The equivalent circuit model.

3.4 Adsorption isotherm

The mechanism of the inhibitor's adsorption on the surface of carbon steel can be described by different adsorption isotherm models. θ is the surface coverage, which is obtained from the corrosion inhibition efficiency η_R, C_{inh} stands for the concentration of the inhibitor, and K_{ads} shows the standard adsorption equilibrium constant. Using the different isothermal equations shown in Table 5 to calculate the linear correlations R^2, the adsorption behaviour of the UHCI-KI on carbon steel interface can be studied accurately [40]. The Langmuir isotherm model was found to be the most appropriate model to fit the results from the electrochemical impedance measurements, with the regression coefficient (R^2 = 0.9977) close to 1. The Langmuir isotherm plot for different concentrations of inhibitor in 4 wt.% citric acid solution is presented in Fig. 6. According to the intercept $1/K_{ads}$ of the straight line in Fig. 6, K_{ads} is calculated as 5.618×10^4 L·mol^{-1}, and the Gibbs free energy ΔG^{θ}_{ads} is calculated as -37.05 kJ·mol^{-1} following Eq. (18) [41]:

$$\Delta G^{\theta}_{ads} = -RTln(55.5K_{ads}) \quad (18)$$

where R is the universal gas constant, T is the temperature and 55.5 is the Molar concentration of water in the solution. A higher K_{ads} and lower ΔG^{θ}_{ads} means that the adsorption reaction can proceed spontaneously, further confirming the strong adsorption performance of the corrosion inhibitors in the citric acid solution and thus exhibiting a better inhibition behaviour [42]. Generally speaking, when ΔG^{θ}_{ads} is higher than -20 kJ/mol, there is an electrostatic adsorption between the corrosion inhibitor and the metal surface, which belongs to physical adsorption. When ΔG^{θ}_{ads} is less than -40 kJ/mol, there is a coordinate bond formed between the inhibitor (unpaired or π electrons) and the metal (the vacant d-orbital) through electron transfer and sharing, which belongs to chemical adsorption [43]. In addition, when the value of ΔG^{θ}_{ads} is between -40 and -20 kJ/mol, this indicates there is a co-existence between the physical adsorption and chemisorption. Hence, with the value of ΔG^{θ}_{ads} being -37.05 kJ/mol, approximately -40 kJ/mol, in this study, the adsorption of the organic molecules on the metal surface belongs to the mixed adsorption mechanism and the chemical adsorption might prevail.

Table 5. Correlation comparison of different adsorption isotherm equations.

Adsorption isotherm model	Equation	Regression coefficient (R^2)
Temkin	$\exp(-2\alpha\theta) = b \times C_{inh}$	0.8221
Freundlich	$\log(\theta) = \log(K_{ads}) + n\log(C_{inh})$	0.8237
Langmuir	$\frac{C_{inh}}{\theta} = \frac{1}{K_{ads}} + C_{inh}$	0.9977

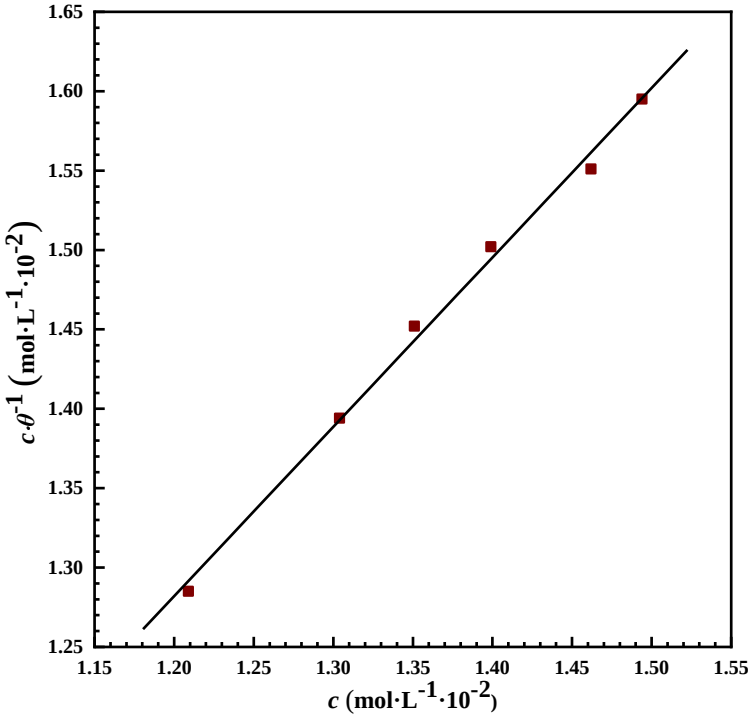

Figure 5. Langmuir isotherm plot for different concentrations of inhibitors in 4 wt.% citric acid solution at 298 K.

In addition, to further investigate the thermodynamic mechanism between the inhibitors and the metal, electrochemical polarisation curves were determined for corrosion inhibition properties at four different temperatures 283 K, 293 K, 303 K and 313 K. The electrochemical parameters obtained by fitting software Versa3 are reported in Table 6. It can be seen in Fig. 7 that there is a good linear relationship between *c/θ* and *c*, and the correlation coefficients using the Langmuir adsorption isotherm model are above 99.99. Similarly, K_{ads} can be obtained from the intercept of the fitted straight line, and ΔH^{θ}_{ads} and ΔS^{θ}_{ads} can be obtained from the line slope and intercept according to Eq. (19) [44]:

$$\Delta G^{\theta}_{ads} = \Delta H^{\theta}_{ads} - T\Delta S^{\theta}_{ads} \quad (19)$$

Table 6. Electrochemical parameters of the carbon steel electrodes in 4% citric acid solution with different ratios of inhibitors after 4 h immersion at 283 K, 293 K, 303 K and 313 K.

Temp, K	UHCI: KI	$-E_{corr}$, V vs SCE	I_{corr}, μA·cm^{-2}	η_p, %	θ
283	0	0.579	57.38	-	-
	39:1	0.449	5.101	91.11	0.9111
	9:1	0.435	4.235	92.62	0.9262
	7:1	0.358	3.730	93.50	0.9350
	4:1	0.449	3.540	93.83	0.9383
	3:1	0.439	2.536	95.58	0.9558
	7:3	0.444	3.248	94.34	0.9434
	5:3	0.440	3.443	94.00	0.9400
293	0	0.573	58.93	-	-
	39:1	0.468	6.016	89.79	0.8979
	9:1	0.484	5.136	91.28	0.9128
	7:1	0.440	4.600	92.19	0.9219
	4:1	0.453	4.416	92.51	0.9251
	3:1	0.443	3.392	94.24	0.9424
	7:3	0.452	4.120	93.01	0.9301
	5:3	0.449	4.332	92.65	0.9265
303	0	0.582	63.60	-	-
	39:1	0.497	6.716	89.44	0.8944
	9:1	0.475	5.775	90.92	0.9092
	7:1	0.462	5.209	91.81	0.9181
	4:1	0.459	4.986	92.16	0.9216
	3:1	0.450	3.892	93.88	0.9388
	7:3	0.455	4.668	92.66	0.9266
	5:3	0.455	4.916	92.27	0.9227
313	0	0.582	89.34	-	-
	39:1	0.463	9.756	89.08	0.8908
	9:1	0.459	8.425	90.57	0.9057
	7:1	0.454	7.567	91.53	0.9153
	4:1	0.445	7.308	91.82	0.9182
	3:1	0.446	5.771	93.54	0.9354
	7:3	0.437	6.879	92.30	0.9230
	5:3	0.433	7.210	91.93	0.9193

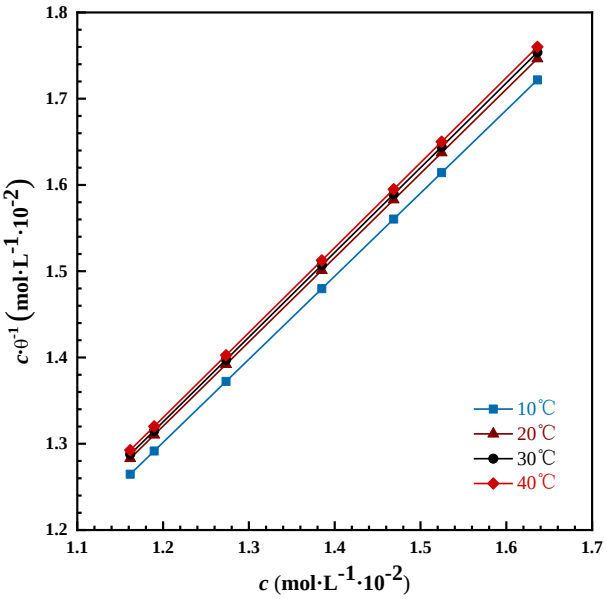

Figure 6. Langmuir isotherm plot for different ratios of UHCI and KI inhibitors in 4 wt.% citric acid solution at 283 K, 293 K, 303 K, 313 K.

The adsorption thermodynamic parameters of the UHCI-KI inhibitor on the surface of carbon steel are shown in Table 7. It can be seen that in the temperature range studied, the corrosion current density increases with temperature in the absence of the inhibitors and the absolute value of ΔG^{θ}_{ads} increases with increasing temperature, indicating that the adsorption capacity of the UHCI-KI inhibitor on the carbon steel surface is enhanced [45]. The enthalpy change $\Delta H^{\theta}_{ads} > 0$ in the adsorption process, and the absolute value of ΔG^{θ}_{ads} is close to -40 kJ/mol, which illustrates that the reaction is an endothermic process and belongs to chemical adsorption. In aqueous solutions, the adsorption of organic molecules is usually accompanied by the desorption of water molecules [46]. The adsorption of organic molecules at the metal/solution interface is considered to be a "Displacement adsorption" phenomenon. Therefore, the positive values of ΔH^{θ}_{ads} and ΔS^{θ}_{ads} can be attributed to the increase of the entropy of the solvent and the increased desorption entropy of water [47]. Moreover, the inhibitory performance of the corrosion inhibitor has little effect in the temperature range of 283 ~ 313 K, mainly related to the concentration ratio of UHCI and KI.

Table 7. The relevant thermodynamic parameters for carbon steel through the Langmuir isotherm model.

Temp, K	ΔG^{θ}_{ads}, kJ/mol	ΔH^{θ}_{ads}, kJ/mol	ΔS^{θ}_{ads}, J/mol·K
283	-34.97	1.279	128.2
293	-36.30		
303	-37.63		
313	-38.80		

3.5 The effect of immersion time on corrosion inhibitors performance

Studying the relationship between the immersion time and corrosion inhibition efficiency is beneficial to understanding the stability of the corrosion inhibitor. In practical applications, this would help to determine the time to replenish the corrosion inhibitor so as to repair the protective film of corrosion inhibitor and reduce the corrosion rate of the metal. In this paper, the impedance spectra of a carbon steel electrode immersed in citric acid solution containing 0.3 wt.% UHCI and 0.1 wt.% KI after 4 h, 8 h and 24 h immersion were determined, and the results are shown in Fig. 8.

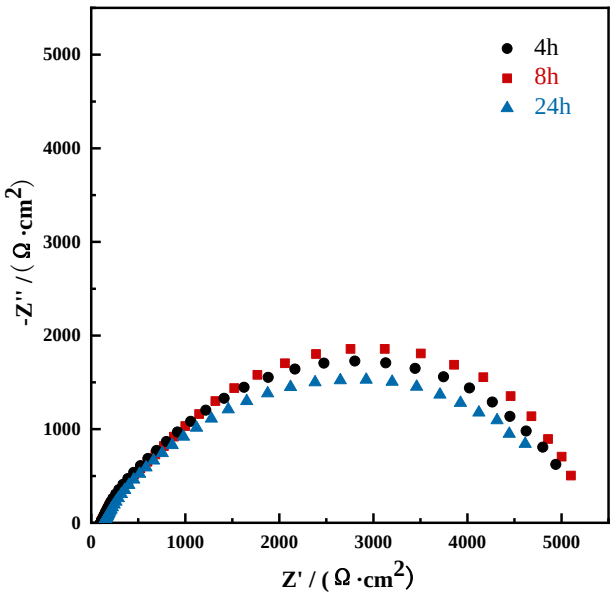

Figure 7. Electrochemical impedance Nyquist plots of the carbon steel electrodes with 0.3% UHCI and 0.1% KI in 4% citric acid solution after different immersion times at 298 K: (a) 4 h; (b) 8 h; (c) 24 h.

Table 8. Electrochemical impedance fitting parameters measured from Figure 8 of 45# carbon steel with 0.3% UHCI and 0.1% KI in 4% citric acid solution after different immersion time at 298 K: (a) 4 h; (b) 8 h; (c) 24 h.

Time, h	R_s, Ω·cm^2	R_{ct}, Ω·cm^2	CPE		η_R, %
			Y_o ($\mu\Omega^{-1}s^n cm^{-2}$)	n	
4	107.2	5652	99.13	0.7079	95.49
8	101.8	5666	111.1	0.7609	95.50
24	117.1	5288	152.4	0.7856	95.18

The relevant data after fitting with Zsimpwin software are listed in Table 8. It can be seen from Fig. 7 and Table 7 that the R_{ct} value of the carbon steel electrode changed little within the range of 4 to 24 h immersion time, indicating that the corrosion inhibition performance of the composite inhibitor was relatively stable within 1 day. According to the guidelines for the Chemical cleaning guide for steam

power plant-DL/T 794-2001, the appropriate control time of citric acid pickling agent is 4 ~ 6 h. Therefore, the corrosion inhibition performance of the UHCI-KI mixed inhibitor is stable within the pickling control time.

3.6 XPS analysis

The chemical composition of the corrosion film formed on the metal surface after 4 h immersion in 4 wt.% citric acid solution containing 0.3% UHCI in association with 0.1% KI, was determined by XPS analysis to identify the interaction between the UHCI/KI inhibitors and the carbon steel surface. The survey and high-resolution spectra of C 1*s*, N 1*s*, O 1s, Fe 2*p* and I 3*d* are shown in Fig. 9 and the relative analytical parameters are reported in Table 9 and Table 10.

The survey spectra shown in Fig. 9a give direct confirmation of the elements of the compounds deposited on the metal surface. The deconvoluted C 1*s* spectrum showed three main peaks (Fig. 9b). The first peak located at 284.6 eV was attributed to C-C and/or C-H aromatic bonds, both were present in the UHCI molecule. The second peak at 285.6 eV was ascribed to C-N and/or C=N^+ species. The third peak was allocated to O=C-O^- and/or C-N^+ bond. The N 1*s* spectrum can be fitted with three contributions (Fig. 9c), the first one at 399.0 eV was assigned to the =N- bond, and the second one at 400.2 eV was assigned to the =N-Fe bond, which indicates that the inhibitor was chemically adsorbed on the metallic surface which agrees with the results from the thermodynamic measurements. Some reports point out that the N-Fe bond complex will prompt a peak shift to a higher binding energy compared to the uncoordinated =N- bond [30].

Similarly, the O 1*s* spectrum of steel surface displayed three doublets (Fig. 9d). The first doublet located at 530.1 eV was attributed to the oxide FeO and Fe_2O_3 species indicating the occurrence of metal corrosion reactions. The second and third doublets at 531.9 eV and 533.4 eV were assigned to the C-O and C=O bonds, respectively. The Fe 2*p* core-level can be resolved with two spin-orbit-split doublets (Fe $2p_{3/2}$ and Fe $2p_{1/2}$), and the Fe $2p_{3/2}$ peak was lying at about 710.4 eV (Fig. 9e). The spectrum can be deconvoluted into two main components centred at 711.2 eV, and 713.6 eV. The peak at a lower binding energy was assigned to the ferric compounds such as FeOOH, Fe_2O_3, and Fe_3O_4, while the other one can be attributed to the presence of a satellite of Fe (III).

In the I 3*d* high-resolution spectra, the peaks at 619.9 eV and 622.0 eV were allocated to the I^- and I_3^-, respectively, which implies the occurrence of partial redox reactions of I^- on the metal surface according to the following Eqs. (20-23) [48]:

$$3I^- \leftrightarrow I_3^- + 2e^- \quad (20)$$

$$2I^- \leftrightarrow I_2 + 2e^- \quad (21)$$

$$2I_3^- \leftrightarrow 3I_2 + 2e^- \quad (22)$$

$$I_2 + 6H_2O \leftrightarrow 2IO_3^- + 12H^+ + 10e^- \quad (23)$$

This XPS analysis confirmed that the steel surface was adsorbed by the inhibitor film and the obtained results show evidence of physical and chemical interactions between the UHCI/KI complex inhibitors and the metal surface.

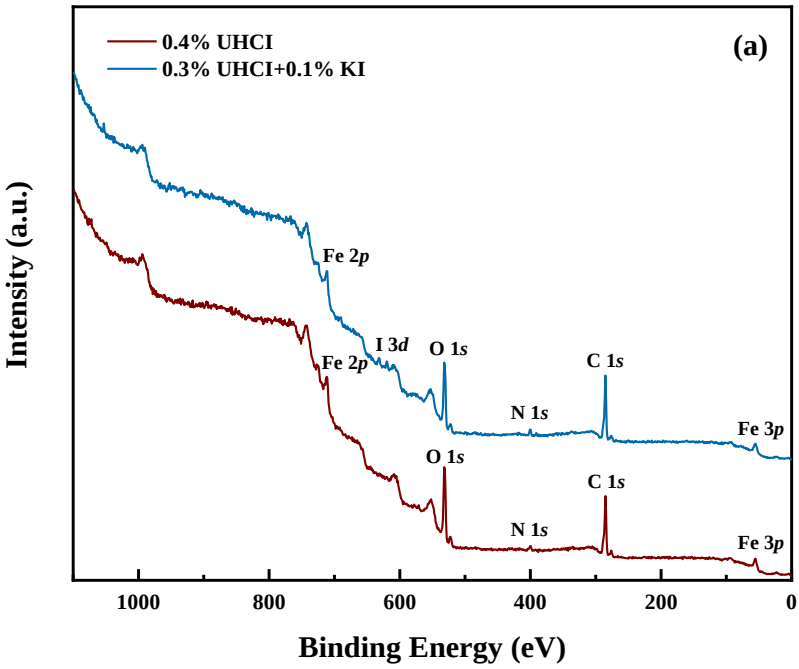

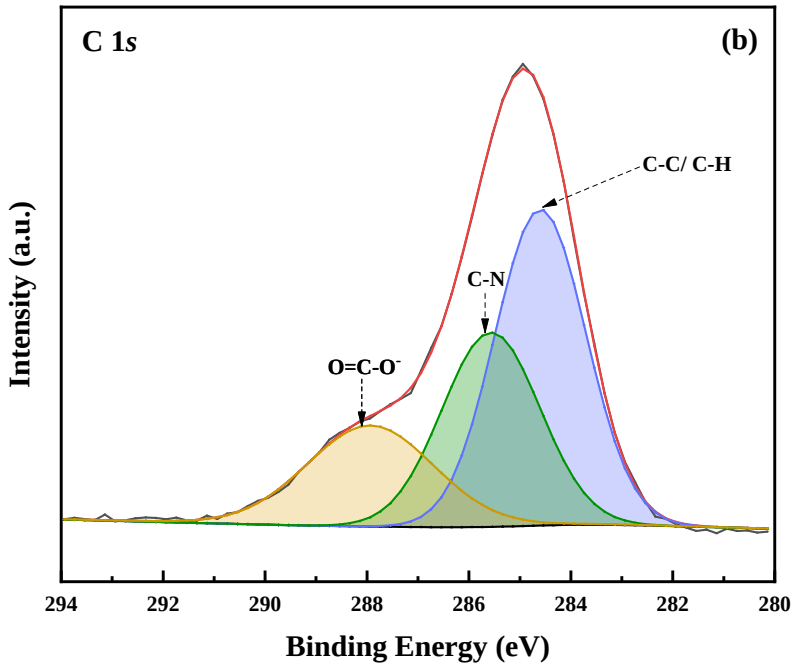

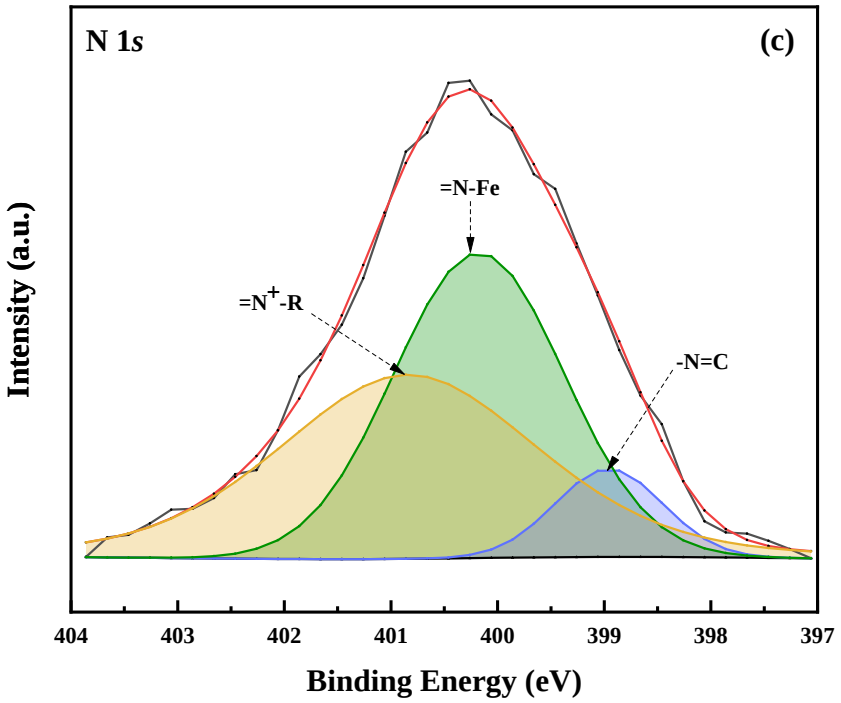
N 1s
(c)
=N-Fe
=N+-R
-N=C
Intensity (a.u.)
404
403
402
401
400
399
398
397
Binding Energy (eV)

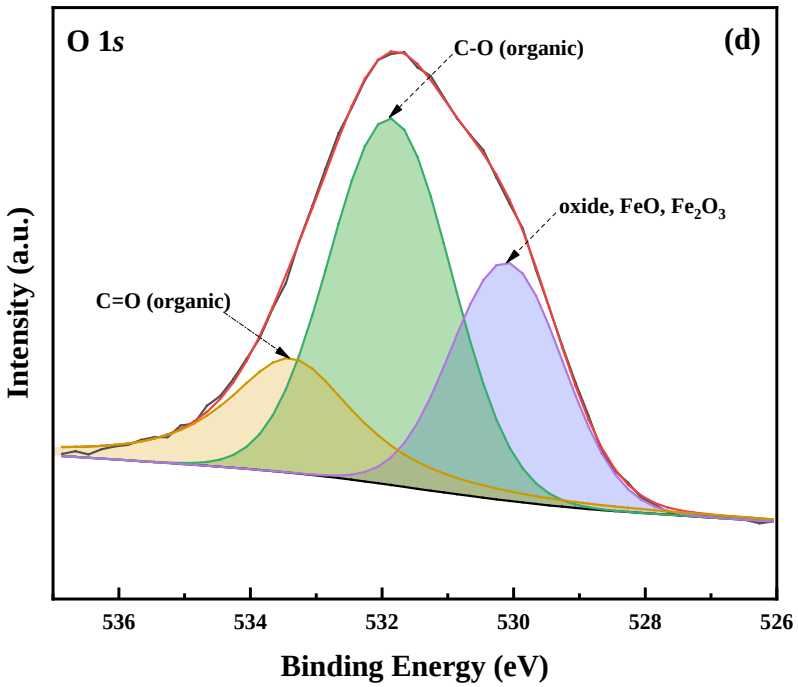
O 1s
(d)
C-O (organic)
oxide, FeO, Fe2O3
C=O (organic)
Intensity (a.u.)
536
534
532
530
528
526
Binding Energy (eV)

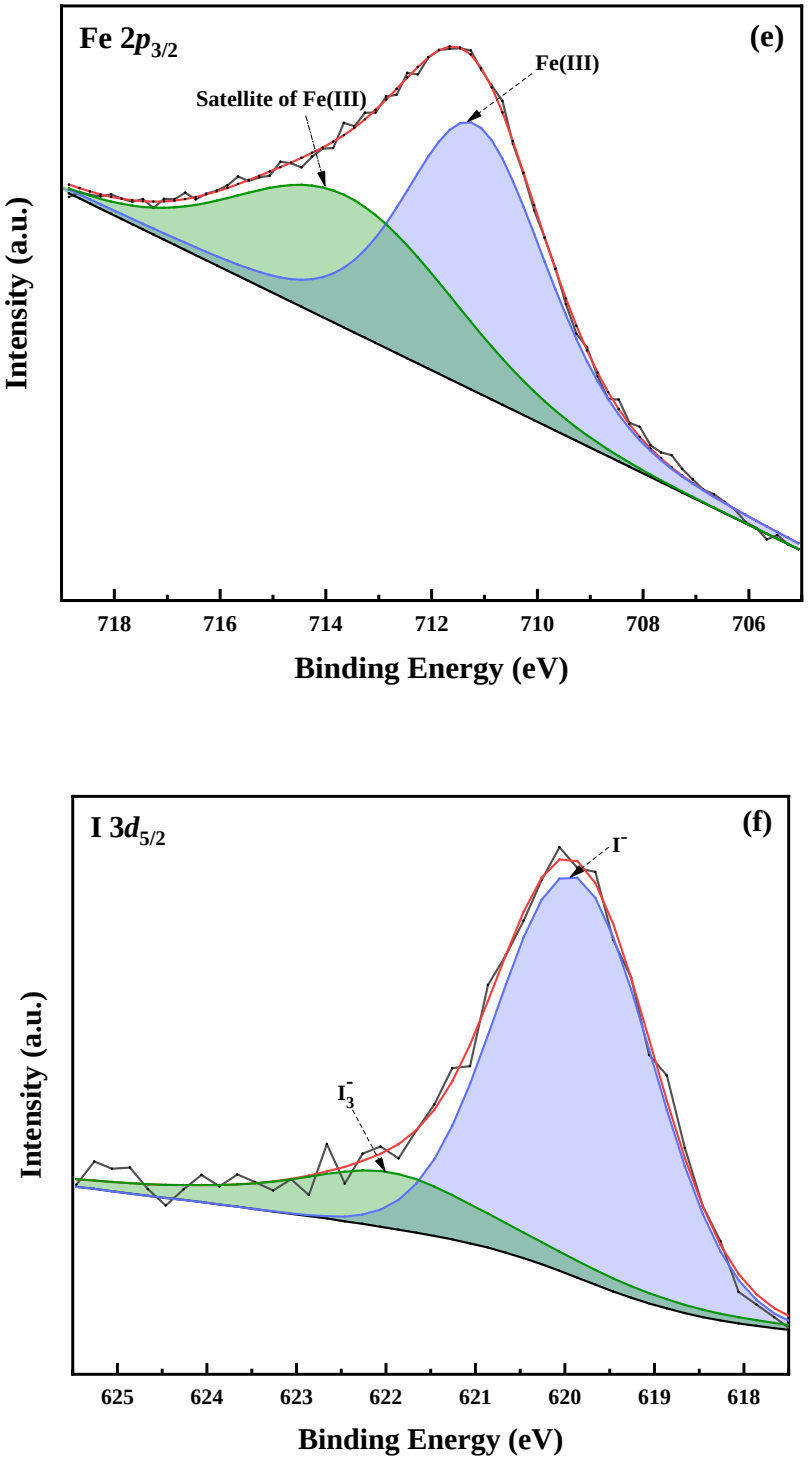

Figure 8. XPS spectra of carbon steel specimen containing 0.3% UHCI and 0.1% KI in 4% citric acid solution after 4 h immersion: (a) The survey scan spectra; (b) C 1*s*; (c) N 1*s*; (d) O 1s; (e) Fe 2*p*; (f) I 3*d*.

Table 9. Binding energies (eV), relative intensity and their possible assignment for the major core lines observed for 0.3% UHCI and 0.1% KI treated carbon steel substrate.

Peak	Position (eV)	Possible assignment	Area ($\times 10^4$)	FWHM (eV)	Ref.
C 1*s*	284.6	C-C/C-H	4.009	2.106	[42] [28]
	285.6	C-N/C=N^+	2.648	2.263	
	287.9	O=C-O-/C-N^+	1.831	2.940	
O 1*s*	530.1	FeO/Fe_2O_3	2.998	2.078	[49]
	531.9	C-O	5.997	2.417	
	533.4	C=O	0.9342	2.570	
N 1*s*	399.0	=N-	0.2212	1.193	[42] [49]
	400.2	=N-Fe	1.208	1.876	
	400.8	=N^+-R	1.244	2.848	
Fe 2$p_{3/2}$	711.2	Fe_2O_3/Fe_3O_4/FeOOH	7.561	3.184	[2]
	713.6	Satellite of Fe (III)	4.845	4.798	
I 3$d_{5/2}$	619.9	I^-	2.555	2.039	[18]
	622.0	I_3^-	0.714	2.756	

Table 10. The atomic percentage of the elemental analyses calculated from XPS survey spectra of carbon steel surface with 0.3% UHCI and 0.1% KI in citric acid medium.

Substrate	Element (at. %)						
	Fe	C	N	O	I	Mn	Si
UHCI-KI treated carbon steel	6.00	62.47	3.18	27.62	0.26	0.10	0.36

3.7. Corrosion inhibition mechanism

The mechanism of corrosion inhibition of the UHCI molecule in the presence of KI at 45# carbon steel surface in a citric acid solution is schematically shown in Fig. 10. From the previous results, UHCI molecules can be adsorbed at the anodic/cathodic sites of the metal surface by physisorption and chemisorption, which can significantly improve the corrosion inhibition efficiency. The surface of metal is often positively charged in acidic solutions due to iron dissolution. The negatively charged iodine ions

are adsorbed on the surface of carbon steel by electrostatic attraction firstly, and then attract the positively charged inhibitor UHCI molecules, which might be by protonation (physical adsorption). Furthermore, the UHCI inhibitor molecules can donate the lone pair electrons on the N, O atoms, and the π electrons on the imidazoline ring, to the unoccupied 3d orbit of Fe (chemisorption), which is also confirmed by the XPS analysis. In addition, I_3^- generated by redox reaction of iodine ions in solution can also play a bridging role. This results in a hydrophobic protective film formed on the metal surface to protect the substrate from erosion.

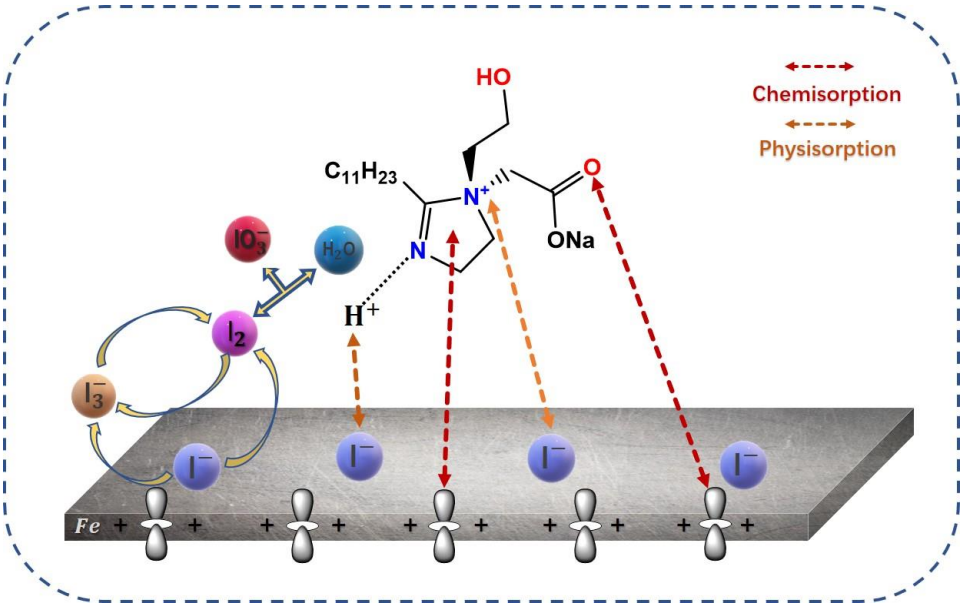

Figure 10. Schematic illustration of adsorption of UHCI molecule in the presence of iodide ions at the carbon steel surface in citric acid solution.

4. CONCLUSIONS

From the above results, the following conclusions can be drawn:

1. The synergistic inhibition efficiency of UHCI and KI on carbon steel corrosion in the 4 wt.% citric acid organic solution was confirmed by the weight loss test and electrochemical measurements

2. When the mass fraction ratio of UHCI to KI was 3:1, η_R reached a maximum of 95.49%, which was in good agreement with the results obtained by the weight loss test and the electrochemical observations.

3. The potentiodynamic polarisation study shows that the UHCI acts as an anodic predominance inhibitor, inferring that the inhibitors forms a barrier film on the metal surface that resists the iron dissolution behaviour.

4. The adsorption of the UHCI, with and without KI, on the surface of carbon steel followed the Langmuir isotherm, and the value of ΔG_{ads}^{θ} was -37.05 kJ mol^{-1}, indicating that it belongs to the mixed adsorption mechanism and the chemical adsorption might prevail, which was confirmed by the

XPS spectral analysis.

DECLARATIONS:

AVAILABILITY OF DATA AND MATERIAL
The raw/processed data required to reproduce these findings cannot be shared at this time as the data also forms a part of an ongoing study.

CONFLICTS OF INTEREST
The authors declare that they have no known competing financial interests or personal relationships that could have appeared to influence the work reported in this paper.

ACKNOWLEDGEMENTS
This work was supported by the Science and Technology Commission of Shanghai Municipality (17DZ2282800 and 19DZ2271100), China.

References

1. D. Bankiewicz, E. Vainio, P. Yrjas, L. Hupa, and G. Lisak, *Fuel.*, 265 (2020) 116886.
2. S. Zhang, L. Hou, H. Du, H. Wei, B. Liu, and Y. Wei, *Corros. Sci.,* 167 (2020) 108531.
3. M. Goyal, S. Kumar, I. Bahadur, C. Verma, and E.E. Ebenso, *J. Mol. Liq*., 256 (2018) 565.
4. P. Dohare, K.R. Ansari, M.A. Quraishi, and I.B. Obot, *J. Ind. Eng. Chem*., 52 (2017) 197.
5. T.J. Harvey, F.C. Walsh, and A.H. Nahlé, *J. Mol. Liq*., 266 (2018) 160.
6. L. Zhang, Y. He, Y. Zhou, R. Yang, Q. Yang, D. Qing, and Q. Niu, *Petroleum.*, 1 (2015) 237.
7. Y. Zuo, L. Yang, Y. Tan, Y. Wang, and J. Zhao, *Corros. Sci.,* 120 (2017) 99.
8. Y.Z. Li, N. Xu, X.P. Guo, and G.A. Zhang, *Corros. Sci.*, 126 (2017) 127.
9. A. Gouron, K. Le Mapihan, S. Camperos, A. Al Farra, V. Lair, A. Ringuedé, M. Cassir, and B. Diawara, *Appl. Surf. Sci*., 456 (2018) 437.
10. Z. Yu, Y. Liu, L. Liang, L. Shao, X. Li, H. Zeng, X. Feng, and K. Cao, *Chem. Phys. Lett*., 735 (2019) 136773.
11. Y. Xiang, Z. Long, C. Li, H. Huang, and X. He, *Int. J. Greenhouse Gas Control.*, 63 (2017) 141.
12. M.M. Solomon, S.A. Umoren, M.A. Quraishi, and M. Salman, *J. Colloid Interface Sci*., 551 (2019) 47.
13. Y. Lu, C. Zhang, W. Wang, and J. Zhao, *Chem. Res. Chin. Univ.*, 35 (2019) 1046.
14. S. Qian, and Y.F. Cheng, *J. Mol. Liq*., 294 (2019) 111674.
15. P. Han, C. Chen, W. Li, H. Yu, Y. Xu, L. Ma, and Y. Zheng, *J. Colloid Interface Sci*., 516 (2018) 398.
16. H. Vashisht, I. Bahadur, S. Kumar, M.S. Goyal, G. Kaur, G. Singh, L. Katata-Seru, and E.E. Ebenso, *J. Mol. Liq*., 224 (2016) 19.
17. Z. Yang, C. Qian, W. Chen, M. Ding, Y. Wang, F. Zhan, and M.U. Tahir, *Colloid Interface Sci. Commun*., 34 (2020) 100228.
18. S. Cao, D. Liu, H. Ding, J. Wang, H. Lu, and J. Gui, *J. Mol. Liq*., 275 (2019) 729.
19. L. Wei, Z. Chen, and X. Guo, *J. Electrochem. Soc*., 164 (2017) C602.
20. P. Singh, D.S. Chauhan, S.S. Chauhan, G. Singh, and M.A. Quraishi, *J. Mol. Liq*., 286 (2019) 110903.
21. P. Singh, D.S. Chauhan, S.S. Chauhan, G. Singh, and M.A. Quraishi, *J. Mol. Liq*., 298 (2020) 112051.
22. M.M. Solomon, S.A. Umoren, M.A. Quraishi, D.B. Tripathy, and E.J. Abai, *J. Pet. Sci. Eng.,* 187 (2020) 106801.

23. I.B. Obot, A. Meroufel, I.B. Onyeachu, A. Alenazi, and A.A. Sorour, *J. Mol. Liq.,* 296 (2019) 111760.
24. J. Wysocka, S. Krakowiak, and J. Ryl, *Electrochim. Acta.*, 258 (2017) 1463.
25. R. Farahati, S.M. Mousavi-Khoshdel, A. Ghaffarinejad, and H. Behzadi, *Prog. Org. Coat*., 142 (2020) 105567.
26. A. Dehghani, G. Bahlakeh, B. Ramezanzadeh, and M. Ramezanzadeh, *J. Mol. Liq*., 279 (2019) 603.
27. C. Verma, E.E. Ebenso, and M.A. Quraishi, *J. Mol. Liq*., 233 (2017) 403.
28. M. Corrales Luna, T. Le Manh, R. Cabrera Sierra, J.V. Medina Flores, L. Lartundo Rojas, and E.M. Arce Estrada, *J. Mol. Liq*., 289 (2019) 111106.
29. C.M. Fernandes, L.X. Alvarez, N.E. dos Santos, A.C. Maldonado Barrios, and E.A. Ponzio, *Corros. Sci.*, 149 (2019) 185.
30. M. Tourabi, K. Nohair, M. Traisnel, C. Jama, and F. Bentiss, *Corros. Sci*., 75 (2013) 123.
31. X. Wang, H. Yang, and F. Wang, *Corros. Sci*., 53 (2011) 113.
32. M. Mu, Y. Chen, D. Yang, A. Yan, and Q. Liao, *Corros. Rev*., 35 (2017).
33. X. Luo, C. Ci, J. Li, K. Lin, S. Du, H. Zhang, X. Li, Y.F. Cheng, J. Zang, and Y. Liu, *Corros. Sci*., 151 (2019) 132.
34. Y. Hao, L.A. Sani, T. Ge, and Q. Fang, *Corros. Sci*., 123 (2017) 158.
35. I.B. Onyeachu, I.B. Obot, A.A. Sorour, and M.I. Abdul-Rashid, *Corros. Sci*., 150 (2019) 183.
36. I.B. Obot, I.B. Onyeachu, and S.A. Umoren, *Corros. Sci*., 159 (2019) 108140.
37. B. Tan, S. Zhang, H. Liu, Y. Guo, Y. Qiang, W. Li, L. Guo, C. Xu, and S. Chen, *J. Colloid Interface Sci.,* 538 (2019) 519.
38. J. Cui, Y. Yang, X. Li, W. Yuan, and Y. Pei, *ACS Appl. Mater. Interfaces.*, 10 (2018) 4183.
39. X. Zheng, S. Zhang, W. Li, M. Gong, and L. Yin, *Corros. Sci*., 95 (2015) 168.
40. S. Pareek, D. Jain, S. Hussain, A. Biswas, Shrivastava, S.K. Parida, H.K. Kisan, H. Lgaz, I.-M. Chung, and D. Behera, *Chem. Eng. J.,* 358 (2019) 725.
41. B.S. Hou, Q.H. Zhang, Y.Y. Li, G.Y. Zhu, H.F. Liu, and G.A. Zhang, *Corros. Sci*., 164 (2020) 108334.
42. M. Corrales-Luna, T. Le Manh, M. Romero-Romo, M. Palomar-Pardavé, and E.M. Arce-Estrada, *Corros. Sci*., 153 (2018) 85.
43. Y. Guo, Z. Chen, Y. Zuo, Y. Chen, W. Yang, and B. Xu, *J. Mol. Liq*., 269 (2018) 886.
44. Z. Hu, Y. Meng, X. Ma, H. Zhu, J. Li, C. Li, and D. Cao, *Corros. Sci*., 112 (2016) 563.
45. O.O. Ogunleye, A.O. Arinkoola, O.A. Eletta, O.O. Agbede, Y.A. Osho, A.F. Morakinyo, and J.O. Hamed, *Heliyon.*, 6 (2020) e03205.
46. W. Zhang, H. Li, A. Wang, C. Ma, Z. Wang, H. Zhang, and Y. Wu, *Mater. Corros*., 71 (2019) 1.
47. A.K. Singh, S. Thakur, B. Pani, B. Chugh, H. Lgaz, I.-M. Chung, P. Chaubey, A.K. Pandey, and J. Singh, *J. Mol. Liq*., 283 (2019) 788.
48. J. Fu, L. Li, D. Lee, J.M. Yun, B.K. Ryu, and K.H. Kim, *Appl. Surf. Sci*., 504 (2020) 144250.
49. M.C. Ismail, S. Yahya, and P.B. Raja, *J. Mol. Liq*., 293 (2019) 111504.